Tetrahedron 133 (2023) 133276

Contents lists available at ScienceDirect

Tetrahedron

journal homepage: www.elsevier.com/locate/tet

A new sulfonamide-based chemosensor for potential fluorescent detection of Cu^{2+} and Zn^{2+} ions

Cephas Amoah [a], Collins Obuah [a, b, *], Michael Kojo Ainooson [a, b], Louis Hamenu [a], Anita Oppong [a], Alfred Muller [b]

[a] Department of Chemistry, University of Ghana, Legon, Accra Ghana
[b] Department of Chemical Sciences, University of Johannesburg, Auckland Park, 2006, Johannesburg, South Africa

ARTICLE INFO

Article history:
Received 14 December 2022
Received in revised form
12 January 2023
Accepted 16 January 2023
Available online 21 January 2023

Keywords:
Fluorescent probes
Quantum yield
Electronic transition
Photophysical properties
Pyrazole derivatives

ABSTRACT

In recent times, there has been an increased demand in the search for probing materials for numerous substances in the environment such as the detection of metals ions. In this study, a new class of pyrazolyl-sulfonamide derivatives of *para*-nitroaniline were synthesized following a multistep approach. The ligands and complexes were characterized using NMR spectroscopy, IR spectroscopy, and mass spectrometry. All the compounds **C1**–**C3** were synthesized in very good yields (85%–92%) and their photo-physical properties measured. All the compounds show fluorescence behaviour with emissions within the UV and far visible range with quantum yields between 7.7% and 25.7%. TD-DFT calculations predictions for the electronic transitions present are in good agreement with experimental observations.

Fluorescent probing studies conducted on the compounds show that **C1**–**C3** were analytically sensitive and possessed significant selectivity towards Cu^{2+} (for **C3**) and Zn^{2+} (for **C1** and **C2**) ions with detection limits between 0.011 and 0.103 mg/L for Cu^{2+} ions and 0.002–0.135 mg/L for Zn^{2+} ions. Overall, **C1** was found to be the most sensitive molecule for the metals studied, having good quantum yield and better selectivity for Zn^{2+} ion compared to Cu^{2+}.

© 2023 Elsevier Ltd. All rights reserved.

1. Introduction

In recent times, research has been geared towards the design of molecules for fluorescent metal detection, recognition and reactivity. This is because, fluorescent materials have found numerous applications as probes, bio-imaging, lasers, and display screens among others [1]. The target therefore has been towards the synthesis of materials with high luminescence properties such as high molar absorptivity, high quantum yield and large stoke shift [2]. The intended application also generally plays a key role in the desired properties, such as deep blue light emitting molecules are desirable for OLEDS with a characteristic shorter wavelength whiles longer wavelength are desirable for molecules intended for imaging purposes.

In this regard, different classes of compounds have been studied, for example single organic fluorophore molecules [3–6] while zeolites [7,8], fluorescent polymers [9], quantum dots [10] and organometallic compounds [11–13] have also been researched for their photophysical properties.

In the use of organic fluorophores, molecules such as fluorescein [14], rhodamine [15,16], acridine [17,18], and oxazine derivatives [19,20] are the most studied groups of compounds. On the other hand, research on fluorescent sulfonamides, primarily focused on the sulfonamide being used as a substituent on an already existing or active fluorophore has also been reported.

Studies on fluorescent probes for metal detection have largely been successful for probing metals such as Fe^{3+}, Fe^{2+}, Cu^{2+}, Zn^{2+}, Hg^{2+}, Pb^{2+}, and Cd^{2+} [21–24]. Other ions like the uranyl ion have also gained attention as a result of contamination from nuclear reaction sites [25]. The capacity of a sensor molecule to detect an ion has been ascribed to numerous reasons, chiefly being the structure of the molecule that is the functional groups present on the molecule, which determines its binding or level of interaction with a metal ion.

In a study conducted by Supuran and coworkers, fluorescein based sulfonamides are used as candidates for the development of imaging and therapeutic strategies in the management of hypoxic tumors which suppress carbonic anhydrase inhibitors [26]. One key

* Corresponding author. Department of Chemistry, University of Ghana, Legon, Accra, Ghana.
E-mail address: cobuah@ug.edu.gh (C. Obuah).

https://doi.org/10.1016/j.tet.2023.133276
0040-4020/© 2023 Elsevier Ltd. All rights reserved.

finding was that the sulfonamide moiety aside its fluorescence enhancement was essential in contributing to the solubility of the fluorophores in water. Another study done by Yin and colleagues, reported the synthesis of naphthalimide-sulfonamide fused dansyl sulfonamide fluorescent probes with dual emission [27]. These molecules were selective in the probing of glutathione of lysosome and capable of tracking them. Also, in a study by Rashatasakhon et al., new sulfonamide-spirobifluorene derivatives were synthesized and found to be good chemosensors with selectivity towards Au(III) ions [28]. It was shown that the sulfonamide portion was key in the complexation of the Au(III) ions which resulted in a quenching of the fluorescent intensity. The range of sulfonamide derivatives as fluorescence materials span from enhance solubility to good probing properties, thus making this class of compounds the potential to be the next generation of fluorescent molecules for imaging or probing materials. Despite all these advances, the application of sulfonamides as central motif as a fluorescence material has not been explored to the best of our knowledge.

Herein, we report on the synthesis of a new family of sulfonamide ligands bearing the pyrazolyl and nitroaniline groups. Their fluorescent properties identify them as blue light emitters and are good selective probes for the detection of Zn^{2+} and Cu^{2+} ions in solution.

2. Results and discussion

2.1. Synthesis of compounds

Compounds **C1**, **C2** and **C3** were prepared from the addition reaction involving *para*-nitroaniline and their respective sulfonyl chloride adducts (Schemes 1) [29]. The formation of the products was guided by stoichiometry addition of the *para*-nitroaniline to a number of sulfonyl chloride moieties with the pyrazole backbone. The compounds were obtained as yellowish brown to brown solids with good yields between 85 and 92%. The compounds were purified by column chromatography, using a solvent system of a mixture of ethyl acetate-methanol in a 7:3 ratio. They were further characterized by IR and NMR spectroscopies, and mass spectrometry.

FT-IR spectroscopy on the compounds showed prominent N–H vibrational peaks showing at around 3431 cm^{-1} and N–O peaks at around 1526 and 1347 cm^{-1} (Fig. S1). The absence of a twin peak usually expected around 3300 cm^{-1} for primary amine and the presence of an N–H corresponding to a secondary amine suggest the formation of the products. ^{1}H NMR spectrum of **C1** showed the presence of an N–H proton peak at 6.61 ppm and aromatic protons integrating for five protons between 8.10 ppm and 8.35 ppm for the phenyl attached to the pyrazole, while the aniline protons were observed as two doublets between 7.00 ppm and 7.80 ppm (Fig. S2). ^{13}C{^{1}H}-NMR also confirmed the formation of **C1** with peaks at 10.65 ppm and 11.14 ppm for the pyrazolyl methyl protons and peaks between 124.47 ppm and 148.22 ppm for the aromatic carbons (Fig. S3).

The ^{1}H NMR spectrum of **C2** show similar patterns as **C1** with additional protons from the aniline group giving total integration of eight protons, indicating addition of the *para*-nitroaniline to the double sulfonated intermediate (Fig. S4 and Scheme 1). ^{13}C{^{1}H}-NMR spectra also showed carbon peaks at 11.1 ppm and 11.9 ppm for the pyrazolyl methyl protons as well as 124.2 ppm–148.2 ppm for the aromatic carbons (Fig. S5). Compound **C3**, on other hand showed the absence of the pyrazolyl proton usually around 6.00 ppm in the ^{1}H NMR spectrum, confirming a double sulfonation on the di-*tert*-butyl pyrazole. Also, the N–H peak was observed at 5.45 ppm with an integration of 2 protons while the anilinic protons showed two doublets at 7.13 ppm and 8.17 ppm each with an integration of four protons (Fig. S6). ^{13}C{^{1}H}-NMR spectra also showed carbon peaks at 28.4 ppm and 33.5 ppm for the pyrazolyl *tert*-butyls as well as 126.4 ppm–156.5 ppm for the aromatic carbons (Fig. S7). In all **C1** was synthesized as having a single sulfonamide group whiles **C2** and **C3** both possessed double sulfonamide groups.

2.2. UV–vis and fluorescent studies

The electronic absorption properties of the sensor molecules **C1**–**C3** were studied at room temperature in methanol.

All the measurement were conducted in methanol between 270 nm and 800 nm with the spectra bands observed in the near ultraviolet region using a concentration of 0.25–0.45 mM. From the spectra, the prominent band was observed at around 370.0 nm for all the molecules synthesized (Fig. 1a) which corresponds to either a π - π^* transition or an n-π^* transition or both which is characteristic of bands resulting from a nitro aniline derivative. Also, it can be deduced that the stoichiometric difference in the molecules had less effect on the overall change in the absorption maxima in the molecules. That is the presence of a double sulfonamide did not result in much change in the wavelength of maximum absorption compared to the single sulfonamide molecule. However, a slight hypsochromic shift was observed that is from 371 nm in **C1** to 370.5 nm and 370 nm in **C2** and **C3** respectively, this could be due to the overall complexity and bulkiness of their structures.

For fluorescent studies of the molecules **C1** – **C3**, it was observed that all the molecules exhibited multiple emission bands within the UV region, the lower visible region, and the upper visible region. Maximum emissions were observed for the molecules when they were excited between 260 nm and 280 nm. As expected, the emission bands of the compounds were weaker in energies compared to their absorption bands which infers that the energy absorbed by the photon was expended in exciting it, hence emitting a lower energy when returning to the ground state. Emissions within the UV region were the most intense and were between 302 nm and 313 nm while an emission wavelength of 605 nm–623 nm were observed closer to the NIR region (Fig. 1b) and were more desirable especially for bio-imaging studies.

Also, emissions within the UV and Visible range suggest that the molecules where blue light to orange light emitters, a feature which is desirable for their use as OLEDs. One peculiar observation was that the presence of a double sulfonamide in **C2** and **C3** resulted in a red shift of the emission wavelength. For example, in **C1** emission observed at 302 nm was found similarly at 313 nm and 305 nm for **C2** and **C3** likewise those found at 605 nm for **C1** were also found at 620 nm and 623 nm for **C2** and **C3** respectively.

The quantum yield of the compounds **C1**–**C3** were also examined using a 1.00 mM concentration of fluorescein in 0.1 M KOH solution as the reference. A concentration range of 0.25–0.45 nM was prepared for the compounds and quantum yield measured at room temperature. The quantum yields of the compounds were observed to be between 7.7% and 25.5%. **C1** and **C2** both exhibiting an appreciable quantum yield of 25.7% and 15.2% respectively while the di-*tert*-butylpyrazole derivative, **C3** had the least quantum yield (Table 1). This can be ascribed to the higher degree of steric present in **C3** and as a result of the stronger electron donating effect of the *tert*-butyl substituent on the pyrazole compared to that from the methyl groups, thus affecting the extent of conjugation in the molecule.

From the quantum yield values of **C1** and **C2**, it can be deduced that they possess a higher propensity of being used to fluoresce incoming light compared to **C3** as the quantum yield represent the probability of a compound to emit fluorescent radiation when returning from a relatively higher excited state. This observation

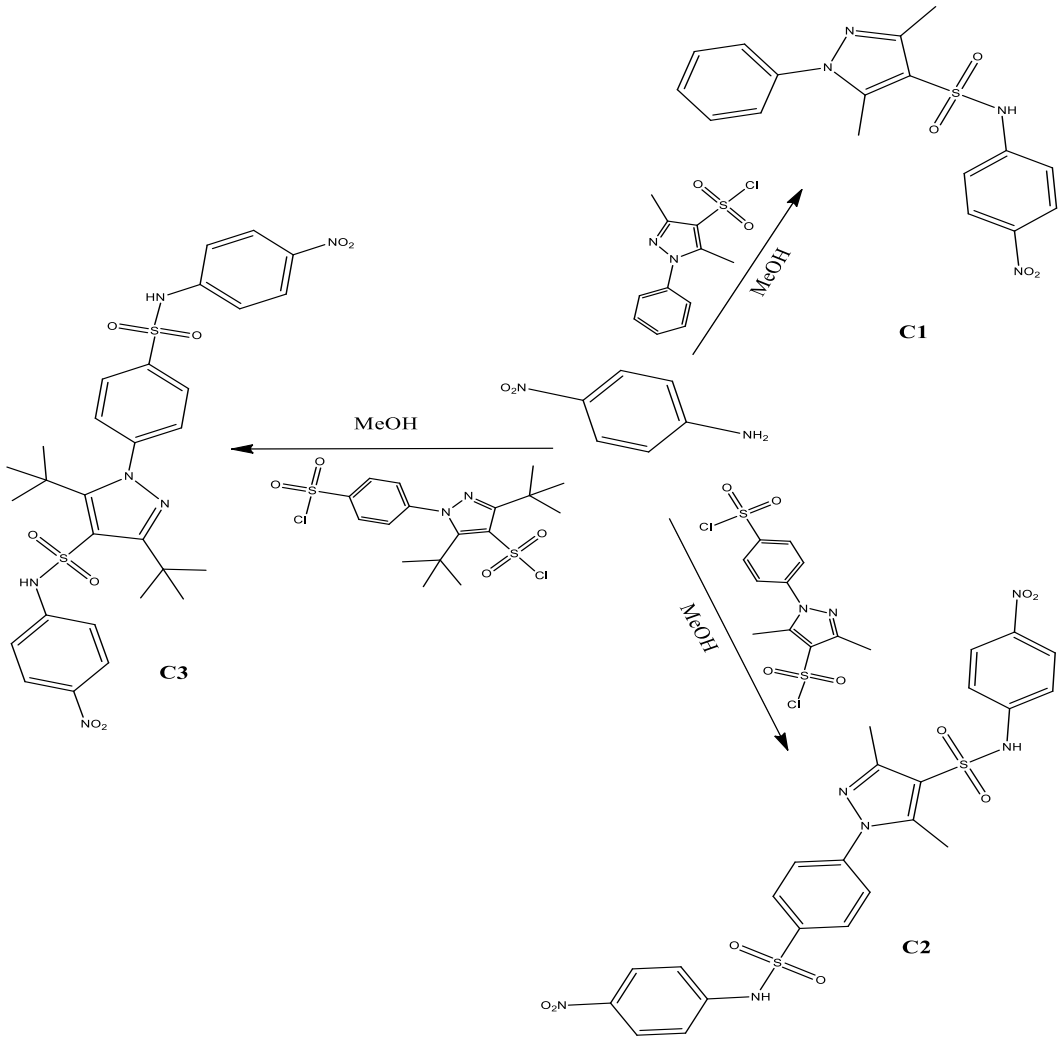

Scheme 1. Synthesis of substituted pyrazolyl sulfonamides, **C1**–**C3**.

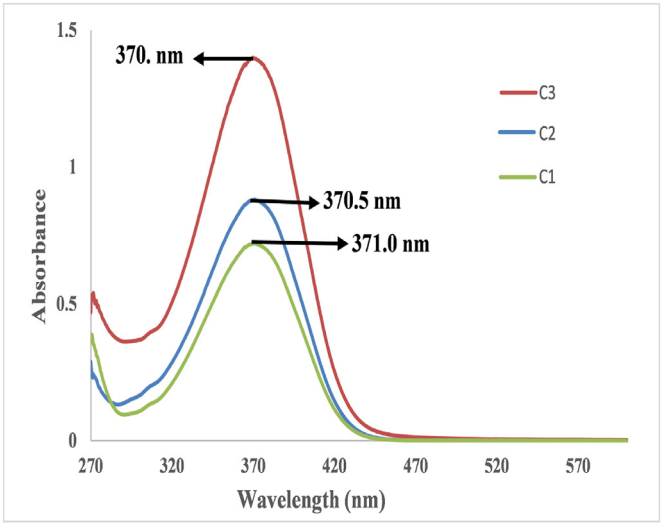

Fig. 1a. UV–Vis absorption Spectra of **C1**, **C2** and **C3**.

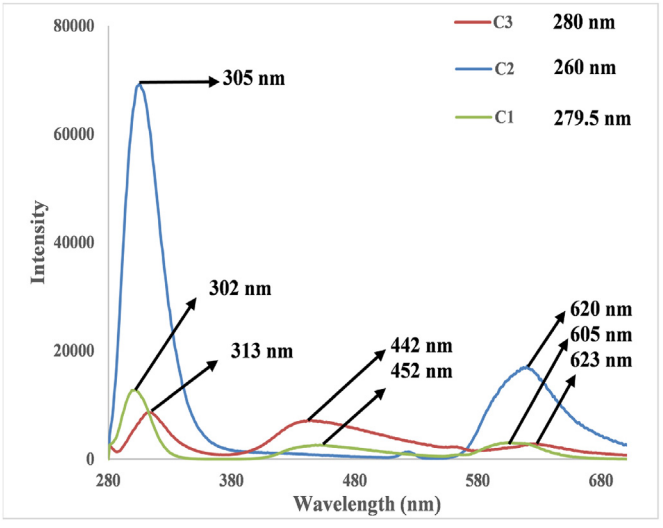

Fig. 1b. Fluorescent spectra of **C1**, **C2** and **C3**.

Table 1
Quantum yield values of C1, C2 and C3.

Compound	Molar Absorptivity (L/mol cm) × 10^3	Quantum Yield (%)
Fluorescein	3.01	93.0
C1	2.15	25.7
C2	3.17	15.2
C3	3.35	7.7

Table 2
Energies of C1–C3 from geometry optimized calculation using B3LYP/6-311G(d,p).

Compound	Energy (Hatrees)	Energy (Kcal/mol)	Energy (KJ/mol)
C1	−1575.687984	−984017.146	−4136968.802
C2	−2615.349382	−1633285.689	−6866599.802
C3	−2851.260355	−1780612.092	−7485984.062

suggests that the compounds can be further explored for use in fluorescent applications including probing purposes.

2.3. Theoretical calculation analysis

DFT calculations were used to determine the energies of the stable minima of the three molecules **C1**– **C3** as well as the UV/Vis spectrum using the B3LYP/6-311G(d,p) level of theory. According to the calculations the molecules were nonlinear at the stable minima (Fig. 2) with the energies presented in Table 2 below; The energies of the *tert*-butyl substituted pyrazole molecule, **C3**, was higher which is expected due to the overall complexity/bulkiness presented by the *tert*-butyl groups.

UV–Vis calculations were computed using the time dependent density DFT theory and the traditional B3LYP functional. The calculated spectra of the molecules corresponded to the experimental in that they both showed single strong absorption with very slight difference in their maximum wavelength from **C1** to **C3** that is 299 nm for **C1**, 305 nm for **C2** and 300 nm for **C3** (Fig. 3) as well as with similar absorption intensities to the experimental spectra (Fig. 1a).

However, the calculated spectra were at lower wavelength with a λ_{max} difference of about 70 nm to which could be attributed to the solvation difference present in the spectra from the experimental measurement. The absorption for **C1** at 299 nm corresponded to an excitation from the ground state to the second excited state (S0–S2) whiles absorptions at 305 nm and 300 nm correspond to S0–S3 and S0–S4 for **C2** and **C3** respectively.

To understand the electronic distribution during the excitation of electrons, the frontier orbitals were also determined from the absorption calculations shown in Fig. 4.

The molecular orbitals of **C1** to **C3** show very similar transitions from the HOMO to the LUMO orbitals and for the HOMO-1 to the LUMO+1 orbitals which are characterized by π –π^* transitions from the phenyl groups and n- π^* from the heteroatoms present. In **C1**, electronic transitions occur from the HOMO/LUMO orbitals around the nitrophenylsulfonamide, while the HOMO-1/LUMO orbitals are the high contributors to the electronic transition in both **C2** and **C3** with electronic transition occurring around the phenyl substitution on the pyrazolyl and the nitrophenylsulfonamide attached.

2.4. Ultra trace analysis

Ultra-trace analysis of Cu^{2+} and Zn^{2+} ions were performed on compounds **C1**–**C3** as they showed good quantum yields. The analysis was conducted using fluorescence spectroscopy and UV–Vis absorbance measurement as a comparable analytical technique. Titration measurements were conducted using a fixed concentration of approximately 20 μM of the sensor molecules and 0–5.00 mg/L of the Zn^{2+} and Cu^{2+} ions.

For sensor molecule **C1**, it was observed that the addition of the Cu^{2+} ions resulted in a decrease in the absorbance which showed that a specie had been attached (Fig. 5a). Similar observation was made when fluorescence measurement was done except that the reduction in the intensity was much significant compared to that from the UV measurement. A further increase in the Cu^{2+} ion concentration resulted in a switch off of the fluorescence of the molecule, **C1** (Fig. 5c).

Hence, it could be deduced that the addition of the Cu^{2+} ion resulted in a quenching of the fluorescence of the molecule **C1**, a

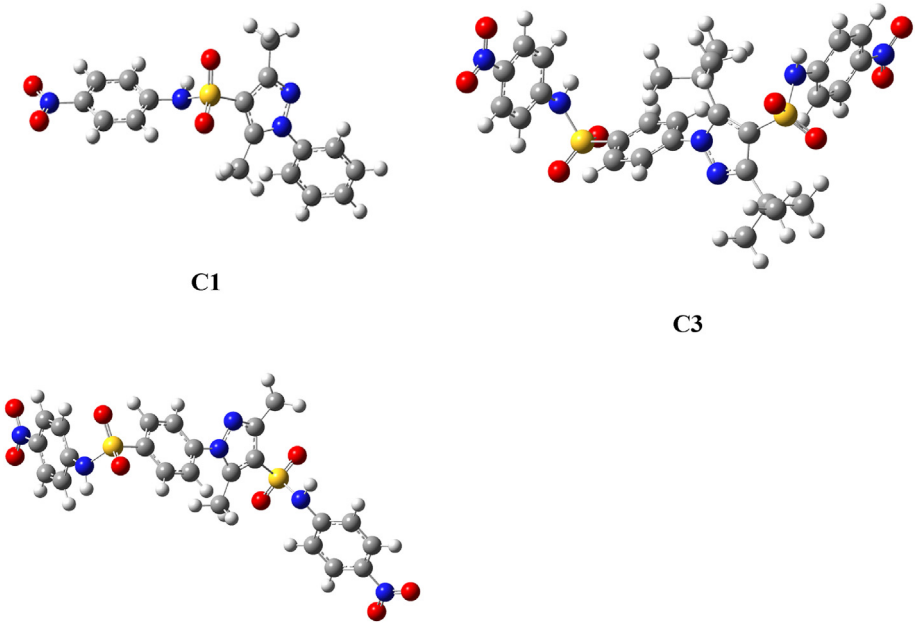

Fig. 2. Geometry optimized structures of C1–C3 using B3LYP/6-311G(d,p).

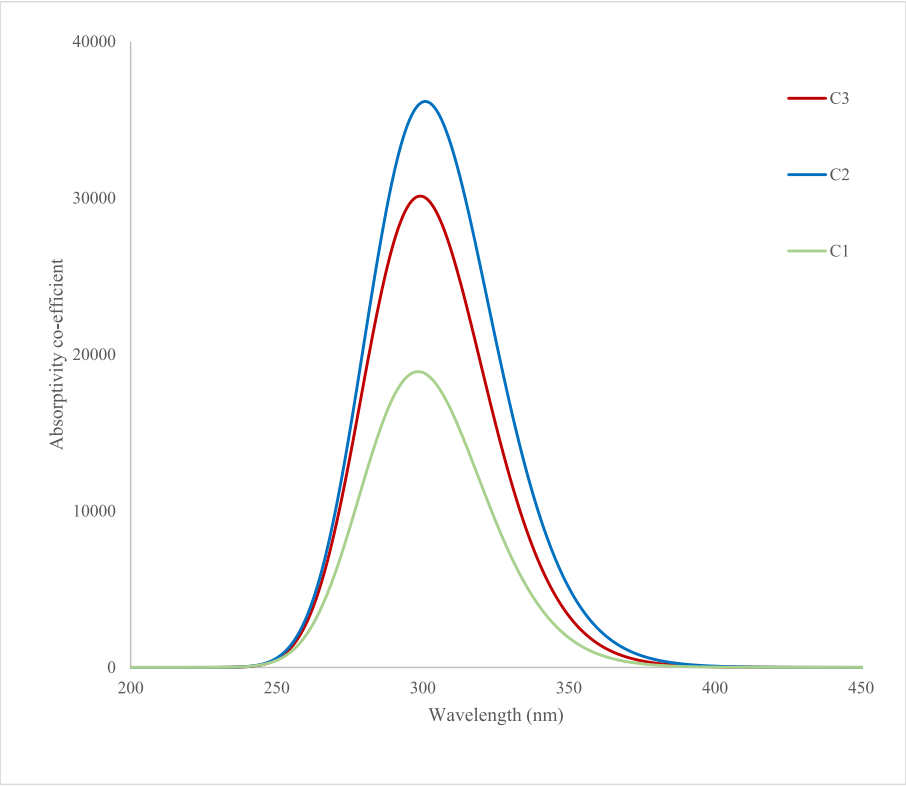

Fig. 3. Calculated Spectra of **C1**–**C3** obtained using the TD-DFT B3LYP/6-311G(d,p) level of theory.

property which is significant of the molecule being used for probing. Zn^{2+} ions on the other hand resulted in a much appreciable increase in the absorbance of **C1** as well as the fluorescence intensity (Fig. 5b and d). Also, the spectra from the addition of both the Cu^{2+} and Zn^{2+} ions revealed that they all exhibited different interactive effect with the sensor molecule **C1** which showed how selective it is towards the two ions.

UV–Vis absorbance measurement for sensor molecule **C2**, also showed similar trend to **C1**, likewise the fluorescence measurement except that the increase in concentration of the metal ions did not result in a switch off of the fluorescent of the molecules (Fig. 6a–d).

For sensor molecule **C3**, addition of both Cu^{2+} and Zn^{2+} ions resulted in an increase of the absorbance (Fig. 7a and b). However, the addition of Cu^{2+} resulted in the formation of new absorbance peak at around 280 nm which was absent in the spectra of the molecule **C3** alone (Fig. 7a). Also, fluorescence measurement revealed a slight increase in the intensity when Zn^{2+} ions were added. However, an increase in the concentration of Cu^{2+} ions resulted in a decrease in the fluorescent intensity, then finally a switch off of the fluorescent of the molecule **C3** (Fig. 7c and d).

These observations revealed that **C3** was a better sensor molecule for probing of Cu^{2+} ions and was also selective. Overall, all the molecules were selective and produced different response especially towards the probing of Cu^{2+} ions.

The mechanism of the sensor molecules as they interact with the Zn^{2+} ions is predicted to occur by a breaking of the Excited State Intramolecular Proton Transfer, ESIPT as the Zn^{2+} ions bind with the sensor molecules leading to an enhanced fluorescence. Whiles the Cu^{2+} ions on the other hand, follows a gradual quenching of the fluorescence emission as the concentration increases, predicted to follow a metal-induced fluorescence quenching approach.

The detection limits of the sensor molecules were estimated from a plot of $(F\text{-}F_o)/F_o$ (where F represent the fluorescent intensity at a particular concentration and F_o represent the fluorescence intensity of the pure molecule) against the concentration of the Cu^{2+} and Zn^{2+} ion concentration at emission wavelength of 302 nm, 305 nm and 313 nm for **C1**, **C2** and **C3** respectively and a linear relation with R^2 between 0.9802 and 1.00 (Figs. S8–S10). The detection limits from both the fluorometric and UV–Vis titrations are tabulated in Table 3.0. From all the sensor molecules, it was observed that the detection limits from the fluorometric titrations were lower than that of the UV–Vis. Hence presented a more analytically sensitive probing tool for the metal ions.

Also, the detection limits for the metal ions were within ranges that are comparable to those reported in literature [30–32]. Overall, the sensors **C1** and **C2** were analytically sensitive toward the determination of Zn^{2+} ions whiles **C3** was more analytically sensitive towards the detection of Cu^{2+} ions.

3. Conclusion

Three pyrazolyl-based sulphonamides sensor molecules were successfully synthesized and characterized following a single pot reaction. Photo-physical studies revealed that the molecules were fluorescent, showing emission bands at the UV and far visible regions. Also, they exhibited good quantum yields, a property which led to a probing study of the compounds on Cu^{2+} and Zn^{2+} metal ions. Probing studies revealed that all the sensors exhibited a rapid response toward increasing concentrations of the metal ions, which was essential for a further development toward their usage as potential probing molecules.

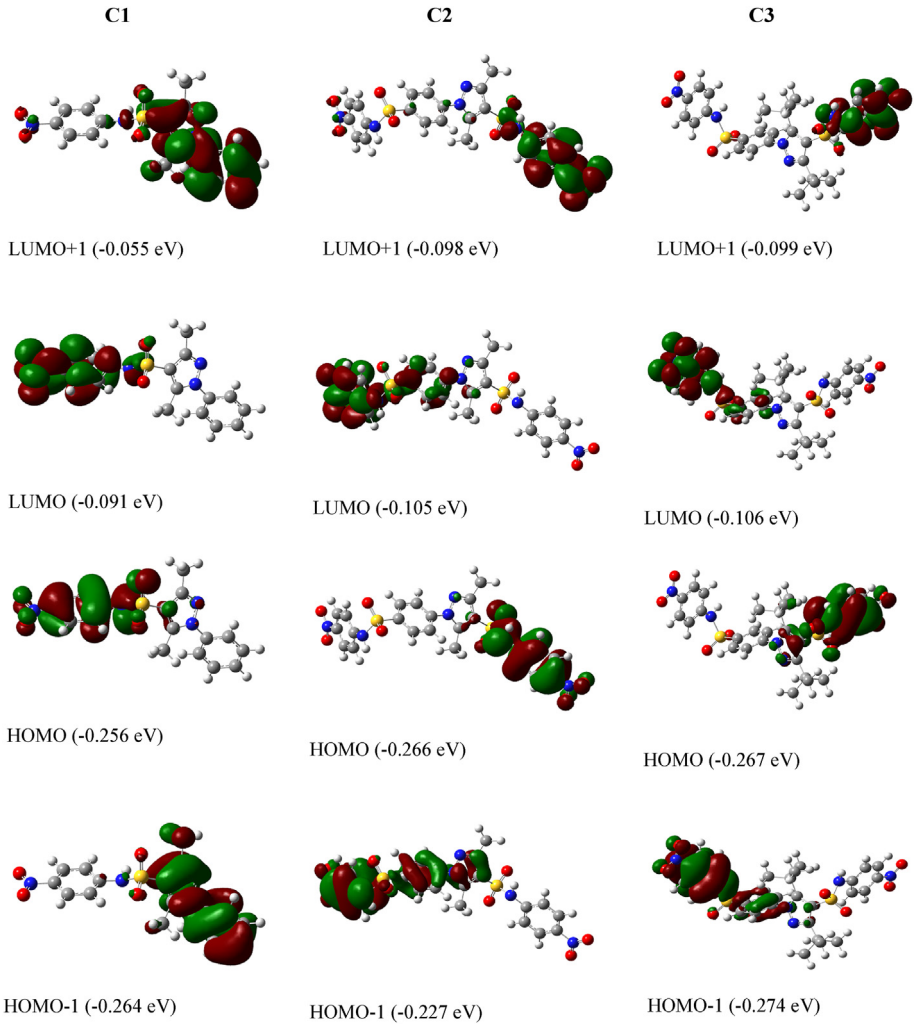

Fig. 4. Frontier Orbitals of C1–C3 from TD-DFT B3LYP/6-311G (d,p) level of theory.

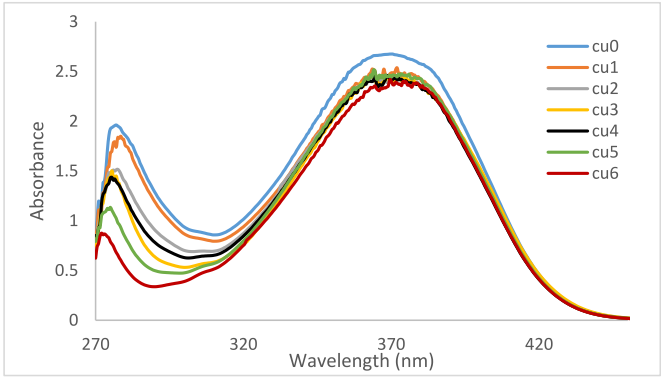

Fig. 5a. UV absorption spectra of C1 and 0–5.00 mg/L of Cu2+ ions.

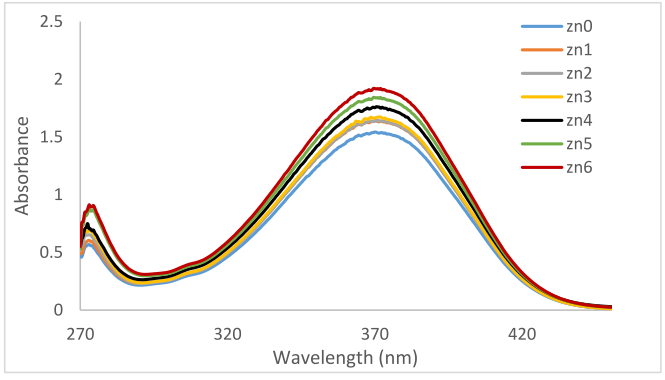

Fig. 5b. UV absorption spectra of C1 and 0–5.00 mg/L of Zn2+ ions.

4. Experimental section

4.1. Materials and methods

Unless otherwise stated, all manipulations were carried out under nitrogen atmosphere using standard Schlenck techniques. All organic solvents were dried and purified by distillation over standard reagents under nitrogen prior to use. Compounds chlorosulfonic acid, phenyl hydrazine, pentane-2,4-dione and 2,2,6,6-tetramethyl-3,5-heptadione, were purchased from Sigma-Aldrich. All chemicals were used as received. Similar methods as reported by us were used for synthesizing the precursors of the sensor molecules [24]. Infrared (IR) spectra of ligands were recorded on a PerkinElmer Spectrum Two equipped with a diamond ATR.

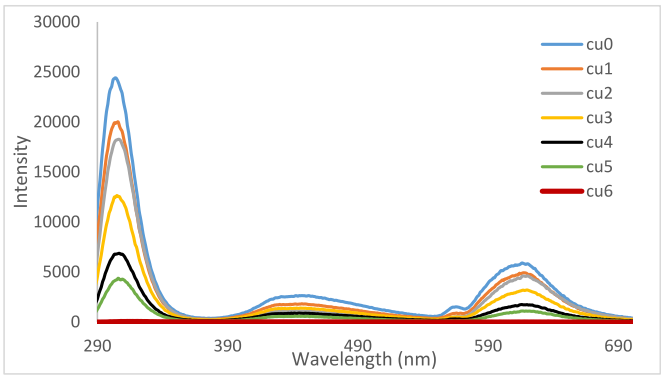

Fig. 5c. Fluorescence spectra of C1 and 0–5.00 mg/L of Cu2+ ions.

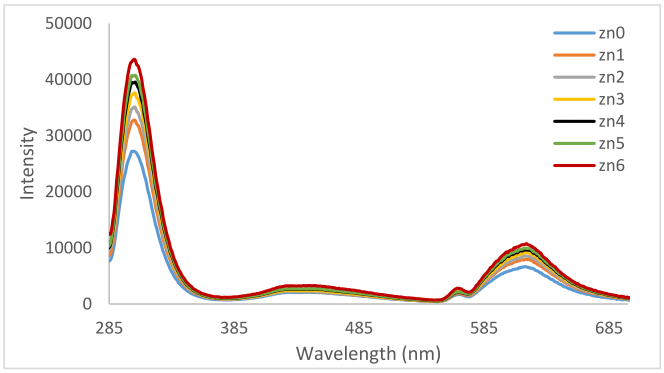

Fig. 5d. Fluorescence spectra of **C1** and 0–5.00 mg/L of Zn^{2+} ions.

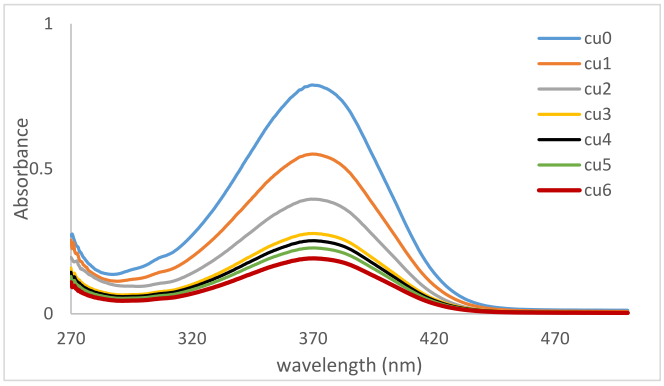

Fig. 6a. UV absorption spectra of C2 and 0–5.00 mg/L of Cu2+ ions.

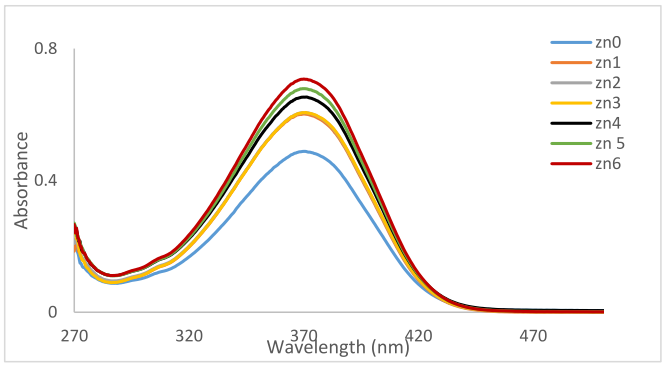

Fig. 6b. UV absorption spectra of C2 and 0–5.00 mg/L of Zn2+ ions.

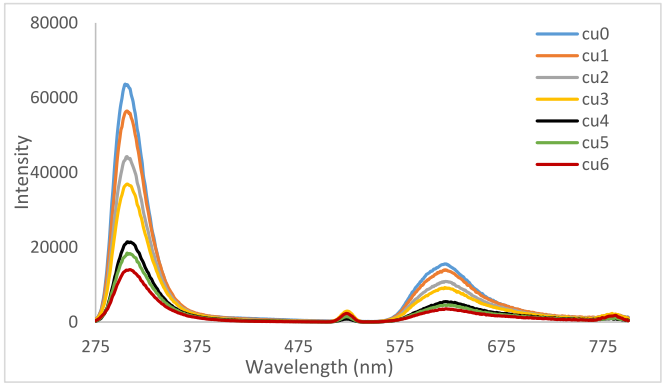

Fig. 6c. Fluorescence spectra of C2 and 0–5.00 mg/L of Cu2+ ions.

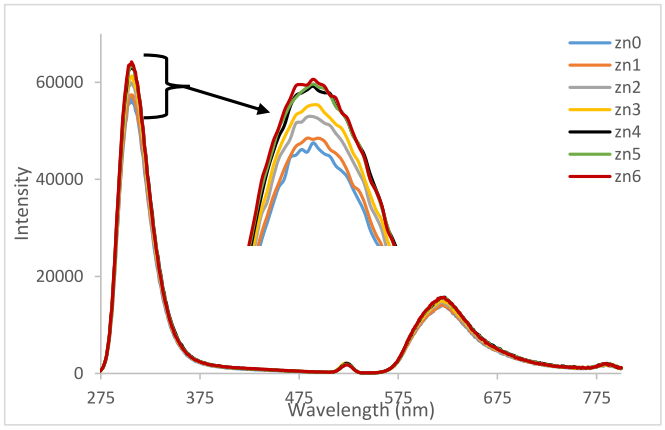

Fig. 6d. Fluorescence spectra of **C2** and 0–5.00 mg/L of Zn^{2+} ions.

Elemental analyses were performed on a Vario Elementar III microcube CHNS. GC-MS analysis of the samples was performed using a PerkinElmer GC Clarus 580 Gas Chromatograph interfaced to a Mass Spectrometer PerkinElmer (Clarus SQ 8 S) equipped with ZB-5HT MS (5% diphenyl/95% dimethyl poly siloxane) fused a capillary column (30 × 0.25 μm ID × 0.25 μm DF). NMR spectra were recorded on a Bruker 500 MHz instrument (^{1}H at 500 MHz and ^{13}C{^{1}H} at 125 MHz) at the Department of Chemistry, University of Ghana. The chemical shifts are reported in δ (ppm) and referenced to the residual proton and carbon signals 3.31 ppm and 49.0 ppm respectively of CD_3OD NMR solvent. Absorption calculations have been performed using the Gaussian 09 program [33] from the CHPC cluster, University of Johannesburg. The ground state geometries were fully optimized using the hybrid B3LYP functional method with the 6-311G(d,p) as basis set. For all optimized structures a frequency analysis at the same level of theory was used to verify that it corresponds to the minimum potential energy surface. For all the minima the number of imaginary frequencies was zero. The absorption and emission properties were calculated using time dependent density functional theory (TD-DFT) in combination with B3LYP hybrid functional with 6-311G(d,p) as basis set.

4.2. Synthesis of compounds

Compounds 3,5-dimethyl-1-phenyl-1H-pyrazole-4-sulfonyl

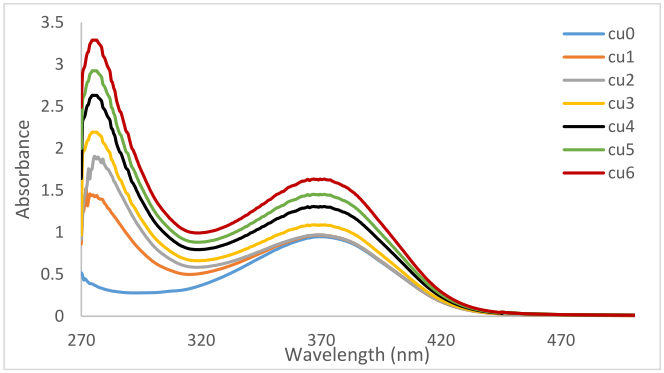

Fig. 7a. UV absorption spectra of C3 and 0–5.00 mg/L of Cu2+ ions.

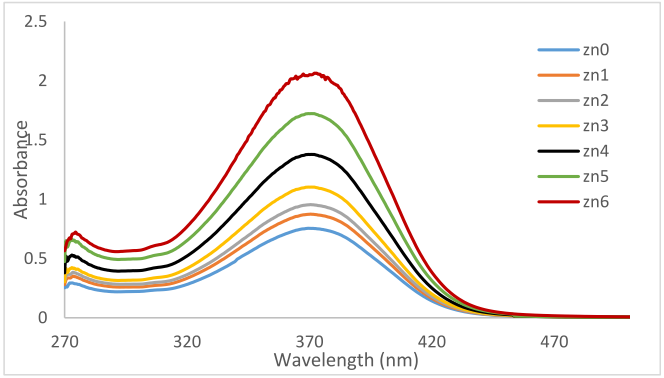

Fig. 7b. UV absorption spectra of C3 and 0–5.00 mg/L of Zn2+ ions.

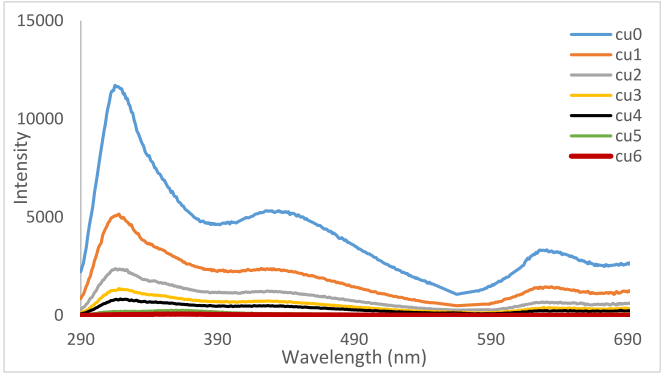

Fig. 7c. Fluorescence spectra of C3 and 0–5.00 mg/L of Cu2+ ions.

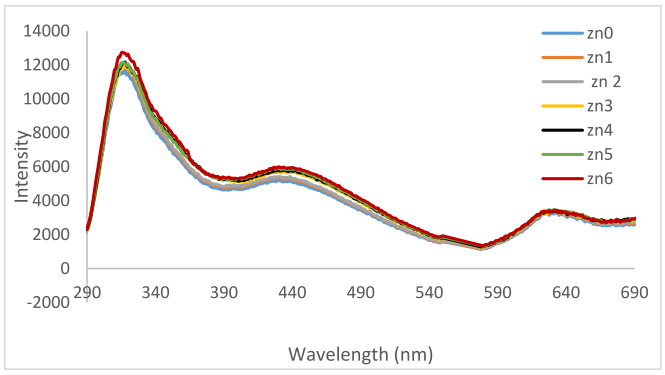

Fig. 7d. Fluorescence spectra of **C3** and 0–5.00 mg/L of Zn^{2+} ions.

chloride, 3,5-di-*tert*-butyl-1-(4-(chlorosulfonyl)phenyl)-1H-pyrazole-4-sulfonyl chloride and 1-(4-(chlorosulfonyl)phenyl)-3,5-dimethyl-1-phenyl-1H-pyrazole-4-sulfonyl chloride were prepared following a multistep procedure as reported previously [29].

4.2.1. Synthesis of 3,5-dimethyl-N-(4-nitrophenyl)-1-phenyl-1H-pyrazole-4-sulfonamide (C1)

An ethanol solution (20 mL) of 4-nitroaniline (0.26 g, 1.85 mmol) was added to a stirring ethanol solution (30 mL) of 3,5-dimethyl-1-phenyl-1H-pyrazole-4-sulfonyl chloride (0.50 g, 1.85 mmol). The resultant mixture was refluxed at 45 °C for 5 h to obtain a yellowish-brown solution. This solution was evaporated to afford yellowish brown solid after column purification using a solvent system of a mixture of ethyl acetate-methanol in a 7:3 ratio. Yield = 0.63 g (92%). ^{1}H NMR (CD_3OD): δ 2.38 (s, 3H, CH_3); 2.51 (s, 3H, CH_3); 6.61 (s, 1H, N–H); 7.12 (d, 2H, $^3J_{HH}$ = 7.5 Hz, Ph); 7.71 (m, 1H, Ph); 7.76 (t, 2H, $^3J_{HH}$ = 8.0 Hz, Ph); 8.07 (d, 2H, $^3J_{HH}$ = 8.0 Hz, Ph); 8.17 (d, 2H, $^3J_{HH}$ = 7.5 Hz, Ph). ^{13}C{^{1}H} NMR (CD_3OD): δ 10.65; 11.14; 109.28; 119.72; 124.47; 126.42; 128.59; 129.37; 131.16; 134.17; 135.47; 142.82; 147.97; 148.22. IR (Diamond ATR, cm^{-1}): 3431 υ(N–H); 1528,1348 υ(N–O). GCMS (EI) *m/z* $[M]^+$ calcd. 372.090: Found: 372.263 (100%). Anal. Calcd for $C_{17}H_{16}N_4O_4S$: C, 54.83; H, 4.33; N, 15.04; S, 8.61%. Found C, 54.95; H, 4.73; N, 15.18; S, 8.41%.

Compound **C2** and **C3** was prepared in a similar manner as described for **C1**, using appropriate reagents.

4.2.2. Synthesis of 3,5-dimethyl-N-(4-nitrophenyl)-1-(4-(N-(4-nitrophenyl)sulfamoyl)phenyl)-1H-pyrazole-4-sulfonamide (C2)

The compound 4-nitroaniline (0.374 g, 2.71 mmol) was reacted with 1-(4-(chlorosulfonyl)phenyl)-3,5-dimethyl-1-phenyl-1H-pyrazole-4-sulfonyl chloride (0.5 g, 1.35 mmol) to give yellowish brown solid. Yield = 0.71 g (91%). ^{1}H NMR (CD_3OD): δ 2.49 (s, 3H, CH_3); 2.51 (s, 3H, CH_3); 7.21 (d, 4H, $^3J_{HH}$ = 8.0 Hz, Ph); 7.58 (d, 1H, $^3J_{HH}$ = 8.0 Hz, Ph); 7.70 (m, 1H, Ph); 8.00 (m, 1H, Ph); 8.07 (d, 1H, $^3J_{HH}$ = 8.0 Hz, Ph); 8.20 (d, 4H, $^3J_{HH}$ = 8.0 Hz, Ph). ^{13}C{^{1}H} NMR (CD_3OD): δ 11.13; 11.19; 11.81; 11.90; 109.30; 109.38; 119.97; 124.23; 124.44; 126.66; 127.04; 127.97; 128.45; 128.47; 128.64; 129.34; 130.58; 131.18; 134.13; 137.03; 138.64; 143.89; 145.72; 147.84; 148.21. IR (Diamond ATR, cm^{-1}): 3431 υ(N–H); 1526,1347 υ(N–O). GCMS (EI) *m/z* $[M+H]^+$ calcd. 573.080: Found: 573.467 (100%). Anal. Calcd for $C_{23}H_{20}N_6O_8S_2$: C, 48.25; H, 3.52; N, 14.68; S, 11.20%. Found C, 48.50; H, 3.64; N, 14.80; S, 11.11%.

4.2.3. Synthesis of 3,5-di-tert-butyl-N-(4-nitrophenyl)-1-(4-(N-(4-nitrophenyl) sulfamoyl)phenyl)-1H-pyrazole-4-sulfonamide (C3)

The compound 4-nitroaniline (0.305 g, 2.21 mmol) was reacted with 3,5-di-*tert*-butyl-1-(4-(chlorosulfonyl)phenyl)-1H-pyrazole-4-sulfonyl chloride (0.500 g, 1.10 mmol) to give dark brown solid. Yield = 0.62 g (85%). ^{1}H NMR (CD_3OD): δ 1.28 (s, 9H, CH_3); 1.40 (s, 9H, CH_3); 5.45 (s, 2H, N–H); 7.13 (d, 4H, $^3J_{HH}$ = 7.0 Hz, Ph); 7.48 (d, 1H, $^3J_{HH}$ = 8.0 Hz, Ph); 7.59 (t, 1H, $^3J_{HH}$ = 7.5 Hz, Ph); 7.78 (s, 1H, Ph); 7.94 (d, 1H, $^3J_{HH}$ = 7.0 Hz, Ph); 8.17 (d, 4H, $^3J_{HH}$ = 7.0 Hz, Ph). ^{13}C{^{1}H} NMR (CD_3OD): δ 28.41; 30.05; 33.48; 34.35; 119.175; 126.38; 126.88; 127.18; 127.67; 129.35; 129.61; 130.93; 143.240; 145.91; 149.42; 156.49. IR (Diamond ATR, cm^{-1}): 3431 υ(N–H); 1529,1347 υ(N–O). GCMS (EI) *m/z* $[M]^+$ calcd. 656.170: Found: 656.315 (100%). Anal. Calcd for $C_{29}H_{32}N_6O_8S_2$: C, 53.04; H, 4.91; N, 12.80; S, 9.77%. Found C, 53.05; H, 5.01; N, 12.89; S, 9.87%.

Table 3.0
Limit of Detection of the Cu and Zn ions from titration with **C1**–**C3**.

Compound	Limit of detection for Cu^{2+} ions		Limit of detection for Zn^{2+} ions	
	UV (mg/L)	Fluorescence (mg/L)	UV (mg/L)	Fluorescence (mg/L)
C1	**0.085**	**0.011**	**0.070**	**0.002**
C2	**0.210**	**0.079**	**0.085**	**0.031**
C3	**0.131**	**0.103**	**0.164**	**0.135**

4.3. UV–vis and fluorimetric determination of Cu^{2+} and Zn^{2+} ions

All spectroscopic measurement were carried out at room temperature. UV–Vis Absorbance measurement were done on a UV-1800 Shimadzu Spectrophotometer whiles fluorescent studies were conducted on an RF-6000 Shimadzu Spectrofluorophotometer. The emission spectra were recorded after the excitation wavelength up to 800 nm. The quantum yield was calculated from the equation:

$$\Phi_X = \Phi_{ST} \times \left(\frac{Grad_X}{Grad_{ST}}\right) \times \left(\frac{\eta_X{}^2}{\eta_{ST}{}^2}\right) \quad \text{(Equation 1)}$$

Where, X and ST refer to the test and the standard samples respectively. Grad refers to the integrated emission intensity, η represents the refractive index of the solvents used for the samples and φ represents the quantum yield. Ultra-trace analysis for Cu^{2+} and Zn^{2+} were conducted by *in situ* titration of a fixed concentration of the sensor molecules **C1**–**C3** with varying concentration of Cu^{2+} and Zn^{2+} (0.00, 0.25, 0.50, 0.75, 1.00, 2.00 and 5.00 mg/L). Fluorescence and UV–Vis measurement were carried on the different analyte concentration in a 1 cm quartz cell respectively at room temperature. All titrations were repeated in triplicates and the limit of detection (LOD) of the ions were determined across the various sensor molecules using a calibration plot of analyte concentration against $(F-F_0)/F_0$ for the fluorescent emission. Where F represent the fluorescent emission intensity of the analyte and test sample and F_0 represent the fluorescent emission intensity of the test sample alone. While the LOD from the UV measurement were determined from a plot of analyte concentration versus the absorbance using the Beer Lambert equation. The LOD was calculated from the equation:

$$LOD = 3.3 \times (S_y \ / \ S) \quad \text{(Equation 2)}$$

where S_y and S represent the standard deviation of calibration curve and the slope respectively.

Declaration of competing interest

The authors declare that they have no known competing financial interests or personal relationships that could have appeared to influence the work reported in this paper.

Data availability

Data will be made available on request.

Acknowledgments

We acknowledge the University of Ghana and the University of Johannesburg for financial support for this project.

Appendix A. Supplementary data

Supplementary data to this article can be found online at https://doi.org/10.1016/j.tet.2023.133276.

References

[1] C.R. Ronda, Luminiscence: from Theory to Applications. Weinhiem, Wiley-VCH, 2008.
[2] K.L. Wong, J.C.G. Bünzli, P.A. Tanner, Quantum yield and brightness, J. Lumin. 224 (April) (2020), 117256, https://doi.org/10.1016/j.jlumin.2020.117256. Available from:.
[3] W. Feng, G. Mao, Q. Li, W. Wang, Y. Chen, T. Zhao, et al., Effects of chromium malate on glycometabolism, glycometabolism-related enzyme levels and lipid metabolism in type 2 diabetic rats: a dose-response and curative effects study, J Diabetes Investig 6 (4) (2015) 396–407.
[4] S. Hisham, H.A. Tajuddin, C.F. Chee, Z.A. Hasan, Z. Abdullah, Synthesis and fluorescence studies of selected N-aryl-2-aminoquinolines: effect of hydrogen bonding, substituents and ESIPT on their fluorescence quantum yields, December 2018, J. Lumin. 208 (2019) 245–252, https://doi.org/10.1016/j.jlumin.2018.12.059. Available from:.
[5] J can Qin, Fu Z. hai, Tian L. mei, Yang Z. yin, Study on synthesis and fluorescence property of rhodamine–naphthalene conjugate, Spectrochim. Acta Part A Mol Biomol Spectrosc 229 (xxxx) (2020), 117868, https://doi.org/10.1016/j.saa.2019.117868. Available from:.
[6] J.B. Grimm, L.M. Heckman, L.D. Lavis, Progress in Molecular Biology and Translational Science, in: The Chemistry of Small-Molecule Fluorogenic Probes, first ed., vol. 113, Elsevier Inc., 2013, pp. 1–34, https://doi.org/10.1016/B978-0-12-386932-6.00001-6. Available from:.
[7] E. Johan, Y. Yamauchi, N. Matsue, Y. Itagaki, H. Aono, Preparation of rare-earth-free luminescent material from partially Ag^{+}-exchanged zeolite X, J Ceram Soc Japan 124 (1) (2016) 70–73.
[8] H. Lin, M. Fujii, Luminescent zeolites, in: C. Belviso (Ed.), Zeolites - Useful Minerals, IntechOpen, Rijeka, 2016, https://doi.org/10.5772/63805. Available from:.
[9] D.M. Mayder, C.M. Tonge, G.D. Nguyen, M.V. Tran, G. Tom, G.H. Darwish, et al., Polymer dots with enhanced photostability, quantum yield, and two-photon cross-section using structurally constrained deep-blue fluorophores, J. Am. Chem. Soc. 143 (41) (2021 Oct 20) 16976–16992, https://doi.org/10.1021/jacs.1c06094. Available from:.
[10] S. Gu, C Te Hsieh, C.Y. Yuan, Y.A. Gandomi, J.K. Chang, C.C. Fu, et al., Fluorescence of functionalized graphene quantum dots prepared from infrared-assisted pyrolysis of citric acid and urea, J. Lumin. 217 (September 2019) (2020), 116774, https://doi.org/10.1016/j.jlumin.2019.116774. Available from:.
[11] M. Thirumal, A. Venkattappan, G. Venkatachalam, Ruthenium(III) 2-(amino-fluoreneazo)phenolate complexes: synthesis, characterization, catalytic activity in amidation reaction and Fluorescence quenching studies, J. Organomet. Chem. 923 (Iii) (2020), 121408, https://doi.org/10.1016/j.jorganchem.2020.121408. Available from:.
[12] Y. He, C. Zhong, Y. Zhou, H. Zhang, Synthesis and luminescent properties of novel Cu (II), Zn (II) polymeric complexes based on 1,10-phenanthroline and biphenyl groups, J. Chem. Sci. 121 (4) (2009) 407–412.
[13] C. Amoah, C. Obuah, M.K. Ainooson, A. Muller, Synthesis, characterization and fluorescent properties of ferrocenyl pyrazole and triazole ligands and their palladium complexes, J. Organomet. Chem. 935 (2021), 121664. Available from: https://www.sciencedirect.com/science/article/pii/S0022328X20305672.
[14] J. Lv, F. Wang, T. Wei, X. Chen, Highly sensitive and selective fluorescent probes for the detection of HOCl/OCl- based on fluorescein derivatives, Ind. Eng. Chem. Res. 56 (13) (2017) 3757–3764.
[15] M. Zhang, C. Shen, T. Jia, J. Qiu, H. Zhu, Y. Gao, One-step synthesis of rhodamine-based Fe3+ fluorescent probes via Mannich reaction and its application in living cell imaging, Spectrochim. Acta Part A Mol Biomol Spectrosc. 231 (2020), 118105, https://doi.org/10.1016/j.saa.2020.118105. Available from:.
[16] P. Ding, J. Wang, J. Cheng, Y. Zhao, Y. Ye, Three N-stabilized rhodamine-based fluorescent probes for Al3+ via Al3+-promoted hydrolysis of Schiff bases, New J. Chem. 39 (1) (2015) 342–348.
[17] F. dos Santos Carlos, L.A. da Silva, C. Zanlorenzi, F. Souza Nunes, A novel

macrocycle acridine-based fluorescent chemosensor for selective detection of Cd2+ in Brazilian sugarcane spirit and tobacco cigarette smoke extract, Inorg. Chim. Acta. 508 (March) (2020), 119634, https://doi.org/10.1016/j.ica.2020.119634. Available from:.

[18] K. Krzymiński, A. Ozóg, P. Malecha, A.D. Roshal, A. Wróblewska, B. Zadykowicz, et al., Chemiluminogenic features of 10-Methyl-9-(phenoxycarbonyl)acridinium Trifluoromethanesulfonates alkyl substituted at the benzene ring in aqueous media, J. Org. Chem. 76 (4) (2011) 1072–1085.

[19] A. Choi, S.C. Miller, Silicon substitution in oxazine dyes yields near-infrared azasiline fluorophores that absorb and emit beyond 700 nm, Org. Lett. 20 (15) (2018) 4482–4485.

[20] A. Paudics, S. Farah, I. Bertóti, A. Farkas, K. László, M. Mohai, et al., Fluorescence probing of binding sites on graphene oxide nanosheets with Oxazine 1 dye, Appl. Surf. Sci. (2021) 541.

[21] M. Fang, S. Xia, J. Bi, T.P. Wigstrom, L. Valenzano, J. Wang, et al., Detecting Zn(II) Ions in Live Cells with Near-Infrared Fluorescent Probes vol. 24, Molecules, 2019.

[22] C. Yin, F. Huo, N.P. Cooley, D. Spencer, K. Bartholomew, C.L. Barnes, et al., A two-input fluorescent logic gate for glutamate and zinc, ACS Chem. Neurosci. 8 (6) (2017 Jun 21) 1159–1162, https://doi.org/10.1021/acschemneuro.6b00420. Available from:.

[23] F. Huo, Q. wu, J. Kang, Y. Zhang, C. Yin, A specific fluorescent probe for zinc ion based on thymolphthalein and it's application in living cells, Sens. Actuators, B 262 (2018) 263–269. Available from: https://www.sciencedirect.com/science/article/pii/S0925400518302090.

[24] L. Li, J. Wang, S. Xu, C. Li, B. Dong, Recent progress in fluorescent probes for metal ion detection, Front. Chem. 1–15 (2022;10(April).

[25] Y. Zhang, L. Sun, Q. Yan, X. Qiu, Y. Cheng, B. Wang, et al., Near-infrared fluorescent probe based on cyanine scaffold for sensitive detection of uranyl ions in living cells and water samples, Microchem. J. 180 (2022), 107619. Available from: https://www.sciencedirect.com/science/article/pii/S0026265X22004477.

[26] M. Ferraroni, B. Cornelio, J. Sapi, C.T. Supuran, A. Scozzafava, Sulfonamide carbonic anhydrase inhibitors: zinc coordination and tail effects influence inhibitory efficacy and selectivity for different isoforms, Inorg. Chim. Acta. 470 (2018) 128–132, https://doi.org/10.1016/j.ica.2017.03.038. Available from:.

[27] Z. Xu, M.X. Zhang, G. Li, X. Chen, S.H. Liu, H. Chen, et al., Naphthalimide-sulfonamide fused dansyl-sulfonamide fluorescent probe for tracking glutathione of lysosome with a dual-emission manner, Dyes Pigments 171 (May) (2019), 107685, https://doi.org/10.1016/j.dyepig.2019.107685. Available from:.

[28] K. Silpcharu, P. Sam-ang, K. Chansaenpak, Journal of Photochemistry & Photobiology , A : Chemistry Selective Fluorescent Sensors for Gold (III) Ion from N -picolyl Sulfonamide Spirobifluorene Derivatives vol. 402, 2020 (August).

[29] C. Amoah, C. Obuah, M.K. Ainooson, C.K. Adokoh, A. Muller, Synthesis, characterization and antibacterial applications of pyrazolyl-sulfonamides and their palladium complexes, New J. Chem. 45 (2021) 3716–3726, https://doi.org/10.1039/D0NJ05143H. Available from:.

[30] R.M. Kamel, A. Shahat, Z.M. Anwar, H.A. El-Kady, E.M. Kilany, A novel sensitive and selective chemosensor for fluorescent detection of Zn2+in cosmetics creams based on a covalent post functionalized Al-MOF, New J. Chem. 45 (18) (2021) 8054–8063, https://doi.org/10.1039/D1NJ00871D. Available from:.

[31] Y. Wang, L. Wang, L.L. Shi, Z Bin Shang, Z. Zhang, W.J. Jin, Colorimetric and fluorescence sensing of Cu2+ in water using 1,8-dihydroxyanthraquinone-β-cyclodextrin complex with the assistance of ammonia, Talanta 94 (2012) 172–177, https://doi.org/10.1016/j.talanta.2012.03.013. Available from:.

[32] Z. Shekari, H. Younesi, A. Heydari, M. Tajbakhsh, M.J. Chaichi, A. Shahbazi, et al., Fluorescence chemosensory determination of Cu2+ using a new rhodamine-Morpholine conjugate, Chemosensors 5 (3) (2017) 1–14.

[33] Gaussian09 RA. 1, Mj Frisch, GW Trucks, HB Schlegel, Ge Scuseria, Ma Robb, JR Cheeseman, G. Scalmani, V. Barone, B. Mennucci, GA Petersson et al., Gaussian. Inc., Wallingford CT. 2009;121:150-166.